Overview of the Experimental Phase Equilibria Studies of the Ni-Sn-S, Cu-Sb-S, Cu-Sn-S, Fe-Sb-As, and Fe-Sn-As Systems

Modassir Akhtar[1], Maksym Shevchenko[2] and Evgueni Jak[3]

1. PhD student, Pyrometallurgy Innovation Centre (PYROSEARCH), School of Chemical Engineering, The University of Queensland, Brisbane, QLD, 4072, Australia, Email: m.akhtar@uq.edu.au
2. Senior Research Fellow, Pyrometallurgy Innovation Centre (PYROSEARCH), School of Chemical Engineering, The University of Queensland, Brisbane, QLD, 4072, Australia, Email: m.shevchenko@uq.edu.au
3. Professor, Pyrometallurgy Innovation Centre (PYROSEARCH), School of Chemical Engineering, The University of Queensland, Brisbane, QLD, 4072, Australia, Email: e.jak@uq.edu.au

Keywords: Ni-Sn-S; Cu-Sb-S; Cu-Sn-S; Fe-Sb-As; Fe-Sn-As; liquidus; solidus; phase diagram

ABSTRACT

This article presents an overview of the experimental phase equilibria studies of S-containing systems (Ni-Sn-S, Cu-Sb-S, and Cu-Sn-S) and As-containing systems (Fe-Sb-As and Fe-Sn-As). These systems improve the prediction capabilities of FactSage in a 20-component "Cu_2O"-PbO-ZnO-FeO-Fe_2O_3-CaO-SiO_2-S-(Al_2O_3-MgO-CrO-Cr_2O_3-Na_2O)-(As, Sn, Sb, Bi, Ag, Au, Ni, Co) system for complex pyrometallurgical operations during both refining and recycling. Experiments involved equilibration at predetermined temperatures (300-1200 °C) with or without preheating, followed by rapid quenching in a brine. Quenched samples were then directly measured using an electron probe microanalyzer. For the Ni-Sn-S system, liquid phases (NiS- and SnS-rich mattes and liquid metal) and solid phases ($Ni_{1+x}Sn$, SnS, Ni_3Sn, FCC-Ni, $Ni_{1-x}S$, NiS_2, Ni_3Sn_4, SnS_2, Sn_2S_3, and β-Ni_3S_2) were observed. A new $Ni_3Sn_2S_2$ phase was found to melt incongruently. For the Cu-Sb-S system, liquid metal, matte, FCC-Cu, digenite, Sb, $CuSbS_2$, Cu_3SbS_3, and Cu_3SbS_4 phases were observed. For the Cu-Sn-S system, liquid metal, matte, digenite, SnS, and Cu_3Sn phases were found at liquidus. Also, the immiscibility gaps spread from 1) the Sn-S binary toward the Ni-rich side in the Ni-Sn-S system, 2) the Cu-S binary toward the Sb-S binary in the Cu-Sb-S system, and 3) the Cu-S binary toward the Sn-S binary in the Cu-Sn-S system. The immiscibility gap in the Cu-Sn-S system is wider than in the Cu-Sb-S system. For the Fe-Sb-As system, liquid metal, $FeAs_2$, $Fe_{1-x}Sb$, Fe_2As, FeAs, $FeSb_2$, and BCC-Fe phases were found. For the Fe-Sn-As system, an immiscibility gap near the Fe-Sn system was observed with liquid metal (Fe-rich and Sn-rich) and $Fe_5(Sn, As)_3$, Fe_2As, FeAs, and $FeAs_2$ phases.

INTRODUCTION

The steady decline in the availability of high-grade ores has led to enhanced interest in metal recovery through recycling (Seitkan et al., 2020). Pyrometallurgy is a proficient route for metal recovery (Rudnik, 2016).

For the Ni-Sn-S system, (Peacock and McAndrew, 1950) reported the Sn isomorph of shandite ($Ni_3Sn_2S_2$) compound. (Bok and Boeyens, 1957) reported Ni_2SnS_4 and $NiSn_2S_4$ compounds. (Brower et al., 1974) reported incongruently melting $Ni_3Sn_2S_2$ compound. (Nitta et al., 1976) synthesised a Ni_3SnS_7 compound.

(Jumas et al., 1977) reported Ni_2SnS_4 compound. (Kusumoto et al., 2001) reported Cu, V, Cr, Mn, Fe, Co, Ni, Sn, and S containing lithium secondary battery, having $Ni_{0.2}Sn_{0.8}S_2$ compounds. (Ma and Beckett, 2018) reported Ni_6SnS_2 compound.

For the Cu-Sb-S system, (Pelabon, 1905) studied the Cu_2S-Sb_2S_3 system. (Groth, 1908) reported Cu_3SbS_3 and $CuSbS_2$ compounds. (Meisner, 1921a) studied the Cu-Sb-S isotherms and reported

Cu_3SbS_3 and $CuSbS_2$ compounds. (Asano and Wada, 1968) reported a miscibility gap at 1200 ℃. (Godovikov and Il'yasheva, 1969) studied the Cu_2S-Sb_2S_3-S system.

(Skinner et al., 1972) studied liquidus of the Cu-Sb-S system. (Gather and Blachnik, 1976) studied the Cu_2S-Sb system. (Chang et al., 1979) reported isotherms of the Cu-Sb-S system. (Karup-Moller, 2000) reported isothermal section of Cu-Sb-S system at 700 ℃. (Braga et al., 2008) studied invariant reactions. (Mammadli et al., 2021) studied the $CuSbS_2$-Cu_3SbS_4-Sb_2S_3 system. (Mammadli et al., 2022a) studied the Cu_3SbS_4-Sb_2S_3-S system. (Mammadli et al., 2022b) studied the $CuSbS_2$-Sb_2S_3-Sb system.

For the Cu-Sn-S system, (Meisner, 1921b) studied the Cu-Sn-S system. (Moh and Ottemann, 1962) studied the Cu-Sn-S system. (Gerlach et al., 1969) reported a Cu-Sn-S phase diagram with 1% Ag at 1200 ℃.

(Khanafer et al., 1974) studied different quasi-binaries, viz. Cu_2S-SnS, Cu_2S-Sn_2S_3, and Cu_2S-SnS_2. (Fiechter et al., 2003) studied quasi-binary Cu_2S-SnS_2. (Pogue et al., 2019) studied isotherms of the Cu-Sn-S system at 25 ℃ and 400 ℃.

For the Fe-Sb-As system, (Landon and Mogilnor, 1933) reported colusite mineral, containing Sb, As, Fe, Zn, Sn, Te, Mo, Cu, S, and traces (Cr and W). (Nurbaev et al., 1981) reported impurities removal from lead by adding Fe powder. (Toguzov et al., 1984) studied the liquidus of the Fe-Sb-As system. (Peterson and Twidwell, 1985) reported removal of As by roasting with pyrite from Sb-As-Bi-Ag-Au-Cu containing lead bullion. (Jurkovic et al., 2019) reported Fe-Sb-As mineral in soils as the Fe-Sb-As-Zn-Pb oxides with few minor elements. (Sorulen et al., 2019) reported Fe-Sb and Fe-Sb-As oxide minerals.

For the Fe-Sn-As system, (Okunev et al., 1975) reported an addition of alloys like ferro-chromium, silico-chromium, and their mixtures improves the recovery of Sn in the Fe-Sn-As alloy. (Chumarev et al., 1979) reported activities of Sn and As and distribution of Sn and As between Fe-Sn-As-(Si-Cr-Mn) alloy and lead. (Mueller et al., 1979) reported tin recovery from ores at 1000-1100℃ by removing As and S. (Kovrigin et al., 1985) reported temperature dependence of dross formation. (Jiang et al., 2011) reported removal of As and Sn from Sn-As containing iron concentrated. (Zheng et al., 2019) reported recovery of Fe and Cu at 1300 ℃ by removing Sn and As through selective oxidation.

No literature about the liquidus and solidus of the Ni-Sn-S and Fe-Sn-As systems was found. For the Cu-Sb-S and Cu-Sn-S systems, literature about liquid-solid phase equilibria along the Cu_2S-Sb_2S_3, Cu_2S-SnS, Cu_2S-SnS_2 joins are mostly available. Therefore, an attention is required towards new technologies for Ni, Sn, Cu, Sb, Fe, and As elements for enhanced refining from complex feeds. So far, without the knowledge of matte-liquid metal phase equilibria, metals can be targeted separately.

The scope of this research was to investigate the liquidus and solidus of the Ni-Sn-S, Cu-Sb-S, Cu-Sn-S, Fe-Sb-As, and Fe-Sn-As systems. This work will support the 20 component "Cu_2O"-PbO-ZnO-FeO-Fe_2O_3-CaO-SiO_2-S-(Al_2O_3-MgO-CrO-Cr_2O_3-Na_2O)-(As, Sn, Sb, Bi, Ag, Au, Ni, Co) system in Cu, Zn, Fe, and Pb smelting (Jak et al., 2023) for enhanced prediction of both complex feeds and products at different extraction stages.

EXPERIMENTAL AND ANALYTICAL METHODOLOGIES

Experimental and analytical methodologies are based on the publication from (Jak, 2012).

Materials

High purity Fe, Cu, Sb, Sn, CuS, Cu_2S, S, Ni, and NiS powders and As lump were used as shown in Table 1 with manufacturer's details. To prevent S evaporation and fast achievement of thermodynamic stable phases, Sb_2S_3, SnS, Sn_2S_3, and SnS_2 master compounds were prepared as explained later.

Table 1 Purity and supplier of elements and a compound as powders.

Element/compound	Purity (%)	Manufacturer

As lump	99.999	Alfa Aesar, USA
Fe	99.998	
Cu	99.9	
Sb	99.999	
Sn	99.85	
CuS	99.8	
Cu_2S	99.5	
S	99.999	Aldrich Chemical Company, USA
Ni	99.99	Sigma Aldrich, Germany
NiS	99.99	Changsha Easchem Co. Ltd., China

Preparation of powder mixtures to pelletizing

The bulk compositions were calculated using the internal FactSage database where 2- or 3-phase assemblages were targeted with a minimum of one liquid phase. The proportion of solid was always lowered by picking a bulk composition to realize equilibration fast with enhanced quenching rate.

A 10g mixture was used for master compounds while a 400mg mixture was used for bulk compositions. These mixtures were made by blending in an agate mortar using a pestle, followed by compression under pressure of ~80-150 bar using a tool steel die.

Apparatus

All experiments were performed in a vertical impervious alumina tube, surrounded by 4 resistance heating elements. Before proceeding to the experiments, a hot zone in the furnace was calibrated at 1000℃±1℃, followed by temperature calibration by using B and R-type thermocouples simultaneously in the air. These thermocouples were calibrated against standard thermocouples, supplied by National Measurement Institute of Australia, NSW, Australia.

Experimental procedure

For better quenching practice, the bottom of the quartz ampoules was expanded by carefully reducing its thickness by controlled heating from all sides in the presence of controlled pressurized air inside. This improves fracturability on quenching.

These modified ampoules were evacuated and sealed in vacuum. Due to the small sample size and the small ampoule in both height (~1.5-2 cm) and weight (4-6 g), an additional weight as a high-temperature corrosion-resistant tube was placed on an ampoule. A Kanthal-D (FeCrAl alloy) wire (diameter = 0.7 mm) was used to hang ampoules inside the hot zone of the furnace. Some length of the wire at the bottom end was always cut to ensure its strength.

Experiments are based on a closed system (controlled by condensed phases). Experiments were performed by hanging the ampoules at a specific temperature (300-1200 °C) in a predetermined hot zone in the air by using Kanthal wire. The test was completed after elapsing a certain time (minimum 1 h for 1200 °C, 2 h for 1100 °C, 4h for 700-1000 °C, 6h for 600 °C, and 2-4 days for 500 °C equilibration temperature,). Equilibration time was determined for a particular system by equilibrating a fixed bulk composition for different time and temperatures. The wire was pulled from the upper side of the tube, causing a free fall under gravity on an alloy cylinder that was immersed in 25% $CaCl_2$ or 25% $MgCl_2$ brine at -20 °C. This resulted in a quick fracture of the ampoule due to load and expanded bottom. Thus, brine was in contact with quenched phases. The samples were cleaned with tap water, followed by cleaning with ethanol, and finally dried in the forced convection oven.

Manufacturing master compounds

Pelletised elemental powders corresponding to the molar ratio of SnS, Sn_2S_3, SnS_2, and Sb_2S_3 master compounds were used. Each mixture was sealed in an ampoule in a vacuum, followed by inserting it in a furnace.

SnS and Sb_2S_3 mixtures were heated from 400 ℃ to 500 ℃ at the rate of 0.5 K/min, followed by equilibration for 3 h and then natural air cooling to room temperature.

Sn_2S_3 mixture was heated from 300℃ to 800℃ at a rate of 0.2 K/min., followed by 3 h of equilibration. After equilibration, the temperature was dropped to 750 ℃ with a rate of 0.5K/min, where it was re-equilibrated for another 1h, followed by cooling to 400 ℃ with a rate of 1 K/min. SnS_2 mixture was heated from 300 ℃ to 790 ℃ with a rate of 0.2 K/min., followed by 71 h of equilibration. After that, the temperature was dropped to 400 ℃ with a 1 K/minute rate. Finally, both Sn_2S_3 and SnS_2 were naturally air-cooled from 400 ℃ to room temperature.

Two-step pre-heating

As sublimation during equilibration retards equilibrium. Therefore, to attain equilibrium fast, it is essential to allow the formation of arsenide before equilibration. Accordingly, preheating at 600 ℃ for 1 h was given for each bulk mixture.

The pre-heating of a bulk mixture at a temperature was given to undergo full or partial melting of bulk composition. This step ensures an accomplished mass diffusion between or among in-contact phases so that only a thermodynamic stable phase form. In this work, Fe-As and Fe-Sb compounds have higher melting points than many equilibration experiments performed. Also, a few experiments (containing master compounds in bulk mixtures) were performed below the melting point of the used master compounds. These are the potential reasons for this uncertainty. Therefore, many samples were given a second pre-heating to ensure fast attainment of equilibrium between or among stable phases.

Analysis of samples

Different faces of a quenched sample were mounted in an epoxy resin. Conventional metallography was performed to get mirror-like polishing, followed by optical microscopy. Before EPMA measurements, optical microscopy provides three information types (i) surface roughness, (ii) abrasive residues, and (iii) phases formed on quenching; checking all of that ensures that samples are ready for EPMA. The samples were kept in a vacuum desiccator most of the time between polishing and EPMA.

Phase identification and microanalyses

Samples were transported to the EPMA lab (CMM, UQ) after observing under an optical microscope, followed by sealing them in a portable vacuum jar. The resin blocks were carbon coated.

Compositions of quenched phases were directly measured using EPMA. Employment of EPMA by using the wavelength dispersive spectrometer increases the accuracy of the composition of the quenched phases as compared to energy dispersive X-ray spectroscopy and bulk wet chemistry methods.

JEOL JXA 8200L EPMA, manufactured by Japan Electron Optics Ltd., Tokyo was used for this study. In each EPMA session, standards were freshly calibrated and were put in every set of experiments as an unknown at the start, intermediate, and end of measurements, depending upon the number of points in a particular set.

Reference standards (Cu K_α, Sb L_α, Fe K_α, and Ni K_α as pure elements, S K_α as $CuFeS_2$, As L_α as InAs, and Sn L_α as SnO_2) were provided by Charles M. Taylor Co., Stanford, CA. SiO_2 as a standard for Si K_α was also added in each set to monitor any contamination due to the usage of ampoules and abrasives.

Probe current = 38nA at an accelerating voltage = 15kV with various probe diameters, ranging from 0 to 200μm were selected for measurement. The selection of probe diameter depends on (i) solid or liquid and (ii) homogeneity and heterogeneity of phase. E.g., solids are mostly homogeneous in each

range of solid solutions or stoichiometric. Hence, any probe diameter is applicable, depending upon the physical size of the phase. However, extensive care was given to select the probe diameter for a liquid for uncertainty minimization of chemical composition as follows:

Depending on the size of the liquid phase area:

If liquid metal of 100μm was observed, then 90μm of probe diameter was considered to measure the liquid metal. Otherwise, new bulk composition was selected, and experiment was repeated.

Quenching quality:

When dendritic structures or precipitates or both was found then grid option was selected with 90μm, 150μm, and 200μm of probe diameter.

Presence of another stable liquid or solid phase:

When excessive proportion of solid or second liquid phase (say matte) was observed, which sometimes causes an insufficient area for the measurement of liquid metal by EPMA. In such cases, bulk composition was modified, and experiment was repeated.

The Duncumb-Philibert ZAF correction integrated with EPMA software was applied. 5-70 points per phase were measured.

After measuring at a particular probe diameter with standards as unknowns, a second correction was performed for each measured element in a stable phase against standard reference material. Copper, antimony, iron, and nickel were corrected against their pure elemental standard, sulphur was corrected against $CuFeS_2$, As was corrected against InAs, and tin was corrected against SnO_2.

Confirmation of equilibrium accomplished with 4-point assessments.

Jak et. al. (Jak, 2012) reported assurance of equilibrium attainment using 4-point assessments of phase equilibria.

Varying equilibration time:

It assists in observing thermal and chemical equilibrium over time. It also ensures the dissolution of any metastable phase that leads to a final and no change in the chemical composition of each phase formed over elapsing time.

Direct measurement of quenched phases to determine homogeneity by using EPMA with WDS:

Measuring using EPMA is the second step in getting confidence in the achievement of equilibration of phases formed during step (a) against their chemical homogeneity. It also reflects a transition from non-equilibrium to metastable and finally equilibrium.

Producing final equilibrium point with different bulk compositions.

It confirms the studied system is approaching thermodynamic equilibrium irrespective of the direction adopted like the different bulk mixtures, different equilibration temperatures with mandatory first preheating and optional second pre-heating of the starting mixture, etc.

Systematic analyses of specific phase equilibrium reactions

It involves in-depth analyses of reactions occurring in the area of temperature interest to confirm both equilibrium achievement and results accuracy. Points 1-3 (varying equilibration time, direct measurement of quenched phases to determine homogeneity by using EPMA with WDS, and producing final equilibrium point with different bulk compositions) lack in confirming the achievement of thermodynamic equilibrium as proximity to an equilibrium point of a system minimizes its driving force to accomplish the same. In many systems, a phase of fixed solid solution or stoichiometry, either cannot be quenched to room temperature or transform into another phase within an hour to months. Sophisticated analytical techniques like EPMA contribute to identifying possible complete or incomplete reactions that occurred during equilibration, followed by their correlations at various temperatures of interest. One possible way is the line analysis of composition by using EPMA.

Further planning to complete analyses

The experimental direction was from liquidus to solidus, where equilibration at high temperature was first done and then advanced towards a lower temperature. This methodology reduces the possibility of the formation of metastable phases. It allows the fast accomplishment of thermodynamic equilibrium and eases the systematic analyses of possible phase equilibria reactions. After analysing the first set of results, further experiments were planned based on 1) target phases and primary phase field, 2) number of phases (minimum two-phase assemblage was selected to move further), 3) the presence of solid fraction and its type, and 4) target phase equilibria reaction. When solid fraction was observed to increase with a decline in equilibration temperature then at some point, the bulk composition was modified.

RESULTS AND DISCUSSIONS

All experimental results were in agreement with the average and standard deviation (mathematically calculated using measured 5 points for the solids and 70 points for the liquids) of measured phases.

Ni-Sn-S system

In this system, liquidus, solidus, boundaries, and primary phases field(s) of liquid phases (NiS- and SnS-rich mattes and liquid metal), MeX ($Ni_{1+x}Sn$), SnS, Ni_3Sn, FCC-Ni, $Ni_{1-x}S$, NiS_2, Ni_3Sn_4, SnS_2, Sn_2S_3, and β-Ni_3S_2 phases were studied with incongruently melting $Ni_3Sn_2S_2$ ternary compound (FIG 1). Here, the immiscibility gap spreads from the Sn-S binary towards the Ni-rich side. Microstructures of different phases are shown in FIG 2(a-h). The point E in the diagrams is eutectic, the point U is peritectic, the point P is quasi-peritectic, the point S is syntectic, the point M is monotectic, and the point Sa is the saddle point.

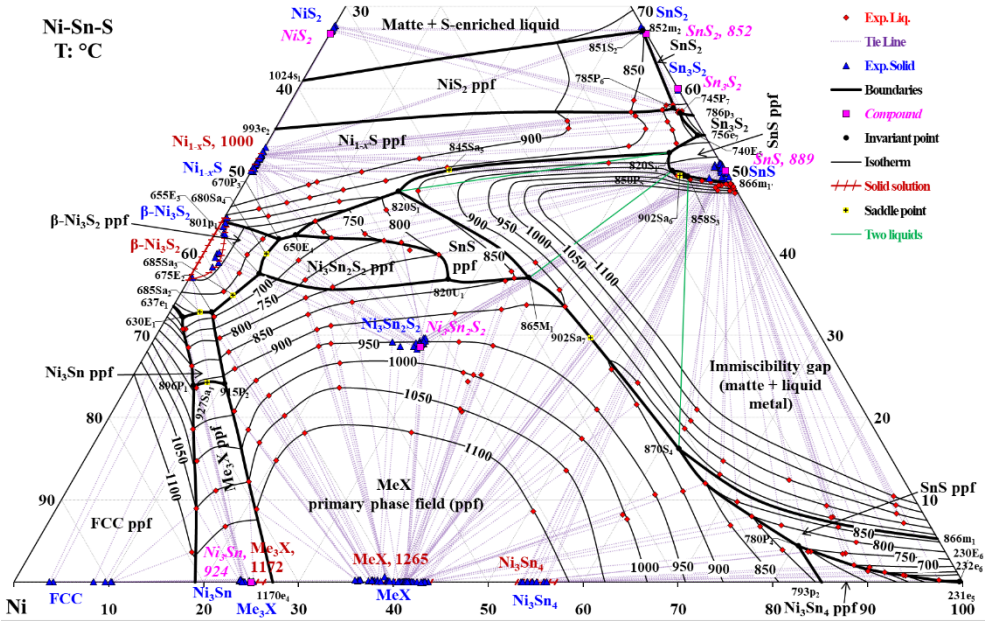

FIG 1 – Ni-Sn-S ternary phase diagram, showing experimental liquids and solids with liquidus, solidus, boundaries, isotherms, and primary phase fields.

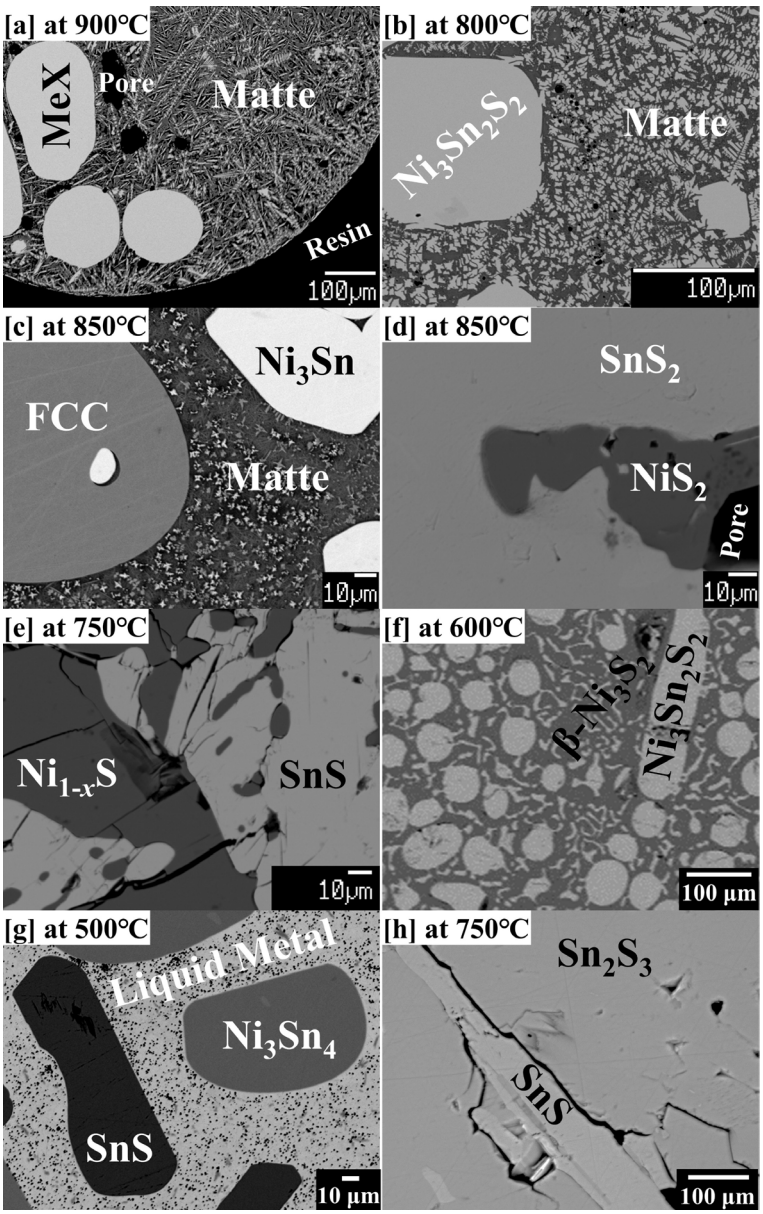

FIG 2 – Microstructures in backscattered electron mode for Ni-Sn-S system, showing (a) matte and MeX, (b) matte and $Ni_3Sn_2S_2$, (c) matte, FCC-Ni, and Ni_3Sn, (d) NiS_2 and SnS_2, (e) $Ni_{1-x}S$ and SnS, (f) $Ni_3Sn_2S_2$ and β-Ni_3S_2, (g) liquid metal, SnS, and Ni_3Sn_4, and (g) SnS and Sn_2S_3 phases.

Cu-Sb-S system

For the liquid metal, matte, FCC-Cu, digenite (Cu_2S_{1+x}), Sb, Cu_3SbS_4, $CuSbS_2$, and Cu_3SbS_3 phases, liquidus, solidus, boundaries, and primary phases fields were investigated (FIG 3). Here, the immiscibility gap spreads from the Cu-S binary towards the Sb-S binary at all compositional ranges of the Cu-Sb binary. Microstructures of phases found are shown in FIG 4(a-c).

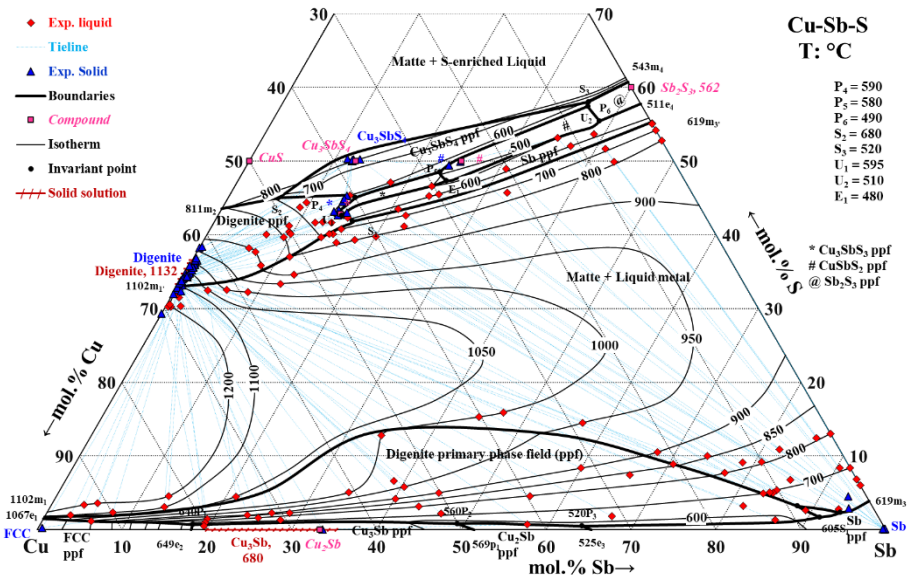

FIG 3 – Cu-Sb-S ternary phase diagram, showing experimental liquids and solids with liquidus, solidus, boundaries, isotherms, and primary phase fields

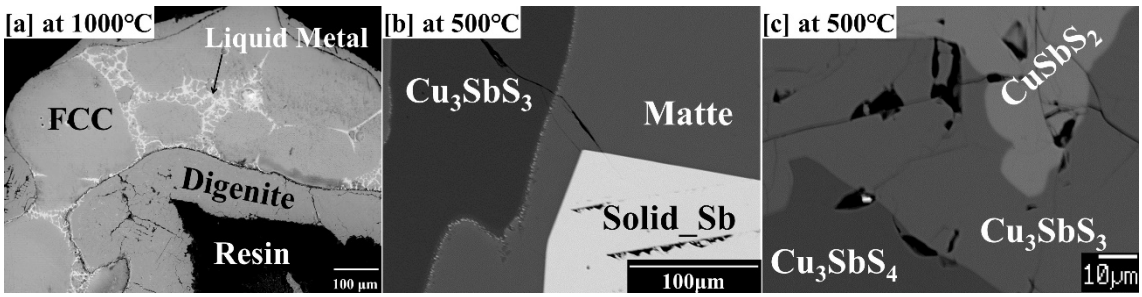

FIG 4 – Microstructures in backscattered electron mode for Cu-Sb-S system, showing (a) liquid metal, FCC-Cu, and digenite (Cu_2S_{1+x}), (b) matte, Cu_3SbS_3, and solid_Sb (c) $CuSbS_2$, and Cu_3SbS_3, and Cu_3SbS_4.

Cu-Sn-S system

For this system, liquidus, solidus, boundaries, and primary phases field(s) of liquid metal, matte, digenite (Cu_2S_{1+x}), SnS, and Cu_3Sn phases were studied (FIG 5). Study of liquidus involving the Cu_2SnS_3, Cu_4SnS_4, $Cu_5Sn_2S_7$, and $Cu_2Sn_3S_7$ ternary compounds is in progress. Here, the immiscibility gap spreads from the Cu-S binary towards the Sn-S binary at all compositional ranges of the Cu-Sn binary, which is wider than the immiscibility gap observed for the Cu-Sb-S system. Microstructures of different observed phases are shown in FIG 6(a-b).

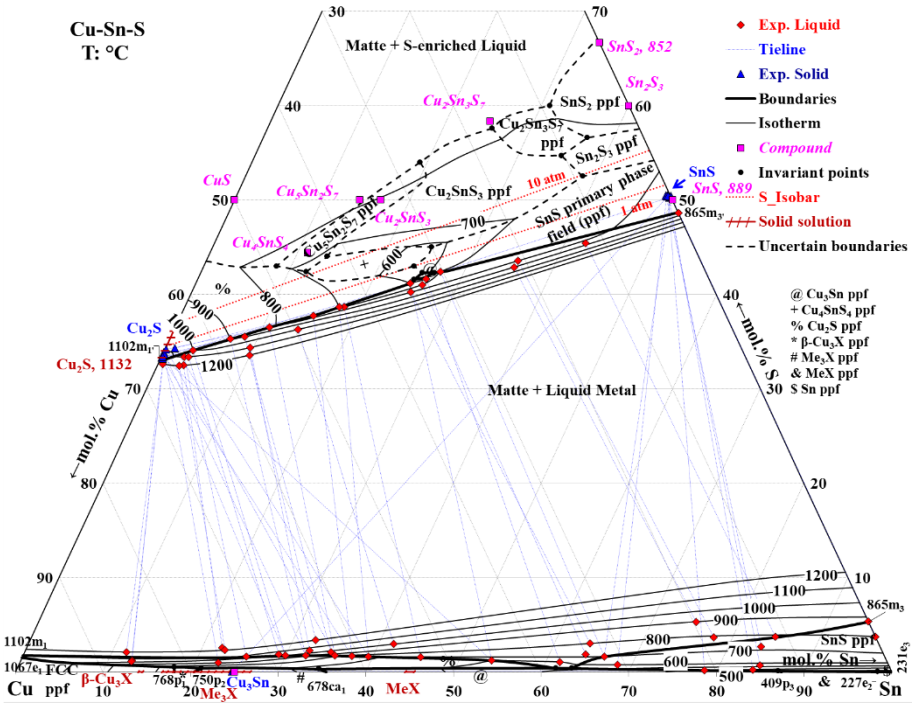

FIG 1 – Cu-Sn-S ternary phase diagram, showing experimental liquids and solids with liquidus, solidus, boundaries, isotherms, and primary phase fields

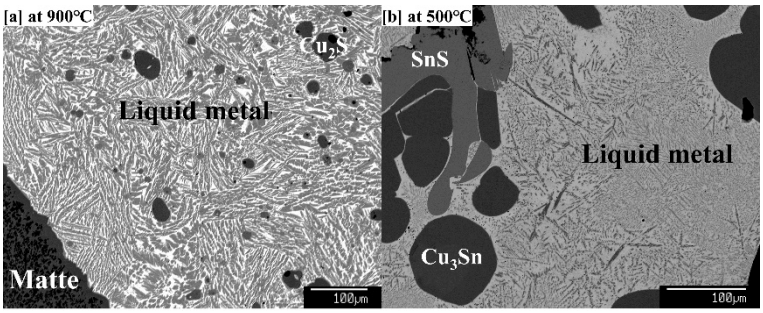

FIG 2 Microstructures in backscattered electron mode for Cu-Sn-S system, showing (a) matte, digenite (Cu_2S), and liquid metal and (b) liquid metal, SnS, Cu_3Sn.

Fe-Sb-As system

In this system, liquidus, solidus, boundaries, and primary phases field(s) for liquid metal, $FeAs_2$, $Fe_{1-x}Sb$ (MeX), Fe_2As, FeAs, $FeSb_2$, and BCC-Fe phases were studied (FIG 7). Here, an immiscibility gap between the Fe_2As-rich and the Sb-rich liquids was found. Microstructures of different phases are shown in FIG 8(a-d).

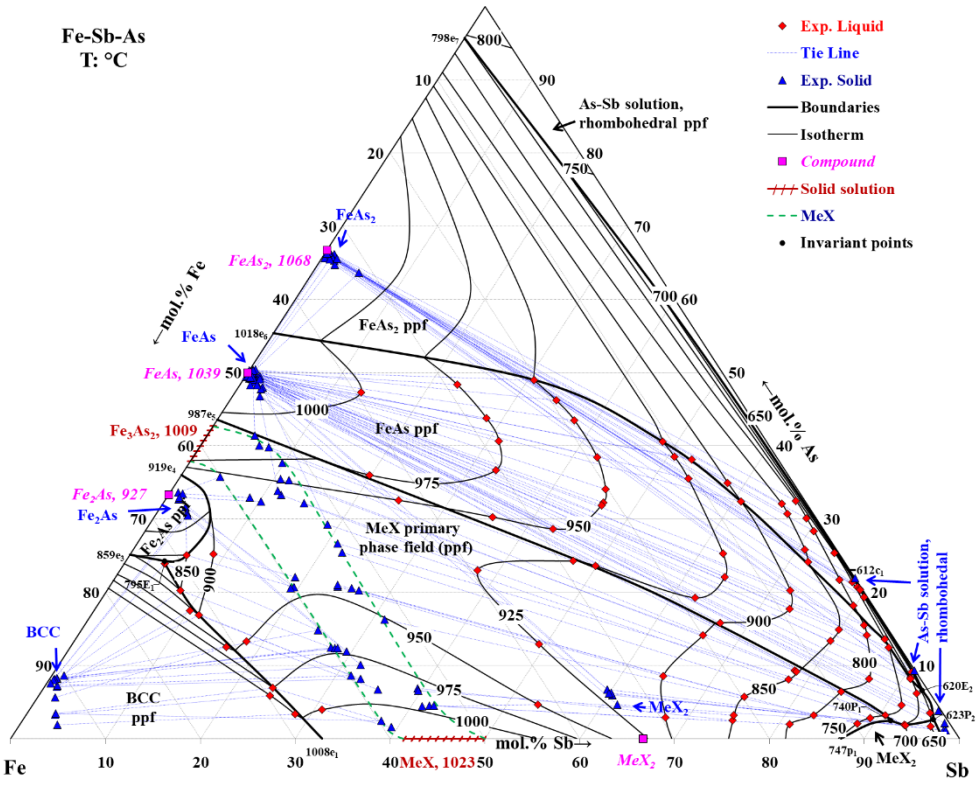

FIG 7 – Fe-Sb-As ternary phase diagram, showing experimental liquids and solids with liquidus, solidus, boundaries, isotherms, and primary phase fields

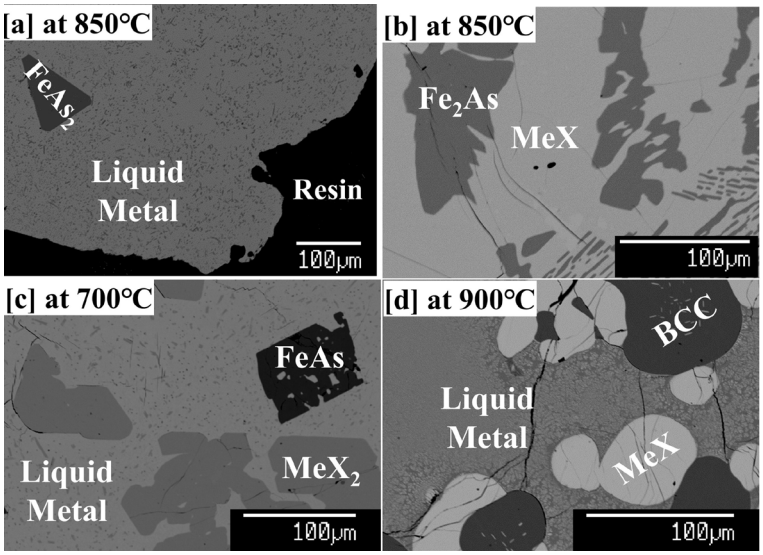

FIG 8 – Microstructures in backscattered electron mode for Fe-Sb-As system, showing (a) liquid metal and $FeAs_2$, (b) MeX and Fe_2As, (c) liquid metal, MeX_2 ($FeAs_2$) and FeAs, and (d) liquid metal, MeX, and BCC-Fe.

Fe-Sn-As system

In this system, liquidus, solidus, boundaries, and primary phases field(s) for liquid metal (Fe-rich and Sn-rich), Me_5X_3 ($Fe_5(Sn, As)_3$), Fe_2As, FeAs, and $FeAs_2$ phases were studied with an immiscibility gap near the Fe-Sn system spreading towards the As-side (FIG 9). Microstructures of different phases are shown in FIG 10(a-d).

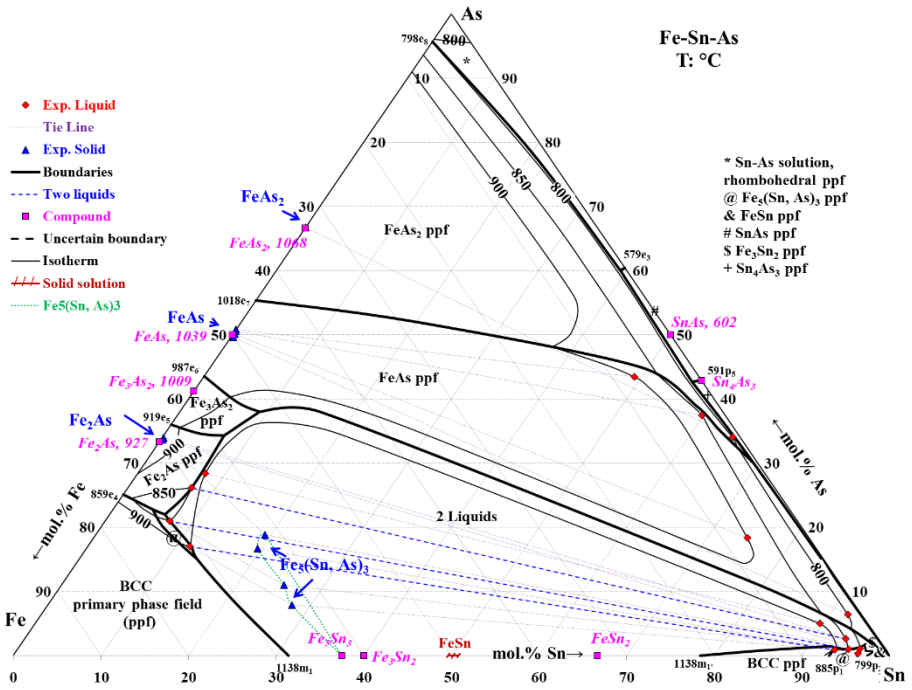

FIG 3 – Fe-Sn-As ternary phase diagram, showing experimental liquids and solids with liquidus, solidus, boundaries, isotherms, and primary phase fields

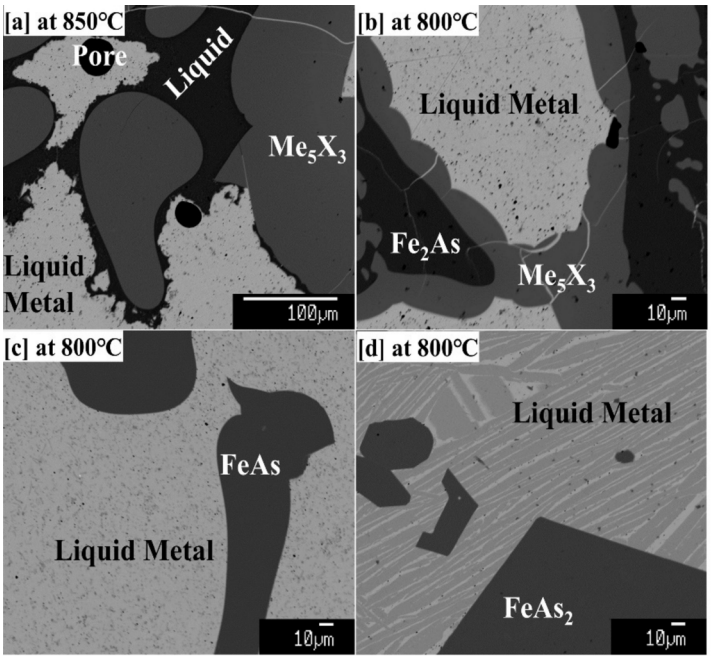

FIG 4 – Microstructures in backscattered electron mode for Fe-Sn-As system, showing (a) liquid metal (Fe-rich) and liquid metal (Sn-rich), and Me_5X_3, (b) liquid metal, Me_5X_3, Fe_2As, (c) liquid metal and FeAs, and (d) liquid metal and $FeAs_2$.

CONCLUSIONS

Phase equilibria of S-containing systems (Ni-Sn-S, Cu-Sb-S, and Cu-Sn-S) and As-containing systems (Fe-Sb-As and Fe-Sn-As) were studied to improve the prediction capabilities of FactSage in a 20-component system for complex pyrometallurgical operations. Different phases for each system were found with their liquidus, solidus, boundaries, and primary phase fields. Different immiscibility gap for each system was observed. The immiscibility gap was the widest for the Cu-Sn-S system among all the studied systems. For the Ni-Sn-S system, two immiscible mattes, liquid metal, $Ni_{1+x}Sn$, SnS, Ni_3Sn, FCC-Ni, $Ni_{1-x}S$, NiS_2, Ni_3Sn_4, SnS_2, Sn_2S_3, β-Ni_3S_2, and $Ni_3Sn_2S_2$ phases were found. For the Cu-Sb-S system, matte, liquid metal, FCC-Cu, digenite, Sb, $CuSbS_2$, Cu_3SbS_3,

and Cu_3SbS_4 phases were found. For the Cu-Sn-S system, liquid metal, matte, digenite, SnS, and Cu_3Sn phases were found. For the Fe-Sb-As system, liquid metal, $FeAs_2$, $Fe_{1-x}Sb$, Fe_2As, FeAs, $FeSb_2$, and BCC-Fe phases were found. For the Fe-Sn-As system, two liquid metals (Sn and Fe-As speiss), $Fe_5(Sn, As)_3$, Fe_2As, FeAs, and $FeAs_2$ phases were observed.

ACKNOWLEDGEMENTS

The authors would like to thank Australian Research Council Linkage program LP180100028 and consortium of copper and lead producers: Anglo American Platinum (South Africa), Aurubis (Germany), BHP Olympic Dam (Australia), Boliden (Sweden), Glencore (Australia), Kazzinc Ltd. (Kazakhstan), Outotec (Finland), Nyrstar (Australia), Peñoles (Mexico), RHI Magnesita (Austria), Rio Tinto Kennecott (USA), and Umicore (Belgium) for the financial support for this study. The authors are very grateful to Prof. Peter Hayes for initiating and contributing to this research program. The authors would like to thank the staff at the Centre for Microscopy and Microanalysis (CMM), The University of Queensland for technical support.

REFERENCES

ASANO, N. & WADA, M. 1968. Distribution of Arsenic, Antimony, and Bismuth between Liquid Copper and Cuprous Sulfide. *Suiyokaishi,* 16**,** 385-388.

BARANOV, A. I., ISAEVA, A. A., KLOO, L. & POPOVKIN, B. A. 2003. New Metal-Rich Sulfides Ni_6SnS_2 and $Ni_9Sn_2S_2$ with a 2D Metal Framework: Synthesis, Crystal Structure, and Bonding. *Inorg. Chem.,* 42**,** 6667-6672.

BOK, L. D. C. & BOEYENS, J. C. A. 1957. Preparation of double metal sulfides of the type AB2S4. II. Compounds of tin. *J. S. Afr. Chem. Inst.,* 10**,** 49-53.

BRAGA, M. H., FERREIRA, J. A., LOPES, C. & MALHEIROS, L. F. 2008. Phase transitions in the Cu-Sb-S system. *Mater. Sci. Forum,* 587-588**,** 435-439.

BROWER, W. S., PARKER, H. S. & ROTH, R. S. 1974. Reexamination of synthetic parkerite and shandite. *Amer. Mineral.,* 59**,** 296-301.

CHANG, Y. A., NEWMANN, J. P. & CHOUDARY, U. V. 1979. *INCRA Series on the Metallurgy of Copper, Phase diagrams and thermodynamic properties of ternary copper-sulfur-metal systems*, International Copper Research Association.

CHUMAREV, V. M., SHOLOKHOV, V. M. & OKUNEV, A. I. 1979. Effect of silicon, chromium, and manganese on tin and arsenic distribution between iron-arsenic-tin melts and lead. *Izv. Akad. Nauk SSSR, Met.***,** 58-61.

FIECHTER, S., MARTINEZ, M., SCHMIDT, G., HENRION, W. & TOMM, Y. 2003. Phase relations and optical properties of semiconducting ternary sulfides in the system Cu-Sn-S. *J. Phys. Chem. Solids,* 64**,** 1859-1862.

GATHER, B. & BLACHNIK, R. 1976. Temperature-composition diagrams in the Cu_2(VIb)-Vb) sections of the ternary copper-(Vb)-(VIb) systems (Vb = arsenic, antimony, bismuth; VIb = sulfur, selenium, tellurium). *J. Less-Common Met.,* 48**,** 205-212.

GERLACH, J., HENNIG, U. & TRETTIN, K. 1969. Distribution of silver to matte and speiss: investigations of the systems copper-cobalt-arsenic-sulfur, copper-iron-arsenic-sulfur, copper-tin-sulfur, copper-arsenic-tin-sulfur. *Erzmetall,* 22**,** 119-122.

GODOVIKOV, A. A. & IL'YASHEVA, N. A. 1969. New data on the copper sulfide-antimony sulfide-sulfur system. *Eksp. Issled. Mineral.***,** 58-60.

GROTH, P. 1908. *Chemische Krystsllographie. 2 Teil. Die anorganischen Oxo und Sulfosalze*.

JAK, E. 2012. Integrated experimental and thermodynamic modelling research methodology for metallurgical slags with examples in the copper production field *9th Intl. Conf. on Molten Slags, Fluxes and Salts.* Beijing, China: The Chinese Society for Metals.

JAK, E., SHISHIN, D., SHEVCHENKO, M. & HAYES, P. C. 2023. University Research, Implementation and Education in support of the Sustainable Metals Production and Recycling. *EMC 2023.* Duesseldorf; Germany.

JIANG, M., SUN, T., QIN, X., JI, Y. & WANG, Z. 2011. Study on removing arsenic and tin from As-Sn bearing iron concentrates by direct reduction roasting with coal. *Kuangye Gongcheng (Changsha, China),* 31**,** 86-89.

JUMAS, J. C., RIBES, M., PHILIPPOT, E. & MAURIN, M. 1977. Preparation and ternary phase characterization of M_2SnS_4 in SnS_2-MS systems. (M = Ti, Cr, Mn, Fe, Co and Ni). *C. R. Hebd. Seances Acad. Sci., Ser. C,* 284**,** 845-847.

JURKOVIC, L., MAJZLAN, J., HILLER, E., KLIMKO, T., VOLEKOVA-LALINSKA, B., MERES, S., GOTTLICHER, J. & STEININGER, R. 2019. Natural attenuation of antimony and arsenic in soils at the abandoned Sb-deposit Poproc, Slovakia. *Environ. Earth Sci.,* 78**,** 672.

KARUP-MOLLER, S. 2000. The Cu-Sb-S phase system at 700°C. *Neues Jahrb. Mineral., Monatsh.***,** 333-336.

KHANAFER, M., RIVET, J. & FLAHAUT, J. 1974. Ternary copper-tin-sulfur. Equilibrium diagrams of the copper(I) sulfide-tin sulfide, copper(I) sulfide+tin(IV), and copper(I) sulfide-tin(IV) sulfide systems. Crystallographic study of the copper-tin-sulfur compounds (Cu_4SnS_4, Cu_2SnS_3, Cu_2Sn_4Sa, and $Cu_4Sn_3S_8$). *Bull. Soc. Chim. Fr.***,** 2670-2676.

KOVRIGIN, V. A., CHURSIN, V. M. & PICHUGIN, B. A. 1985. Dross formation on melts of copper and its alloys. *Tsvetn. Met. (Moscow)***,** 79-82.

KUSUMOTO, Y., FUJIMOTO, M. & FUJITANI, S. 2001. *Secondary lithium battery using mixed sulfide as active mass*. JP patent application.

LANDON, R. E. & MOGILNOR, A. H. 1933. Colusite, a new mineral of the sphalerite group. *Am. Mineral.,* 18**,** 528-533.

MA, C. & BECKETT, J. R. 2018. Nuwaite (Ni_6GeS_2) and butianite (Ni_6SnS_2), two new minerals from the Allende meteorite: Alteration products in the early solar system. *Am. Mineral.,* 103**,** 1918-1924.

MAMEDOVA, N. A., RAGIMOV, S. S., SADYKHOV, F. M. & ALIEV, I. I. 2012. Preparation and physicochemical study of nickel(II) thiostannate in the $NiCl_2$-SnS_2-H_2O system. *Russ. J. Inorg. Chem.,* 57**,** 160-162.

MAMMADLI, P. R., GASIMOV, V. A. & BABANLY, D. M. 2022a. Phase relations in the Cu_3SbS_4-Sb_2S_3-S system. *Chemical problems,* 1**,** 40-47.

MAMMADLI, P. R., GASIMOV, V. A., MASHADIYEVA, L. F. & BABANLY, D. M. 2022b. Phase relations in the $CuSbS_2$-Sb_2S_3-Sb system. *New Mater., Compd. Appl.,* 6**,** 37-43.

MAMMADLI, P. R., MASHADIYEVA, L. F., GASIMOV, V. A., DASHDIYEVA, G. B. & BABANLY, D. M. 2021. Phase Relations in the $CuSbS_2$-Cu_3SbS_4-Sb_2S_3 System. *Azerbaijan Journal of Chemical News,* 3**,** 100-108.

MEISNER, K. L. 1921a. The equilibrium between metal-pairs and sulfur. III. The system copper-antimony sulfur. *Met. Erz,* 18**,** 410.

MEISNER, K. L. 1921b. The Equilibrium between metal-pairs and sulfur. V. The system copper-tin-sulfur. *Met. Erz,* 18**,** 466-468.

MOH, G. H. & OTTEMANN, J. 1962. New investigations of stannite and related minerals. *Neues Jahrb. Mineral., Abh.,* 99**,** 1-28.

MUELLER, L., TRINKS, W., BRAND, K. H. & BEHRENDT, H. P. 1979. Development of tin production at the VEB Mining and Metallurgical Plant Albert Funk at Freiberg. *Neue Huette,* 24**,** 374-378.

NITTA, T., HAYAKAWA, S., KASAHARA, Y. & HIRAKATA, T. 1976. *Sulfide-ceramic bodies*. DE patent application.

NURBAEV, M., TOGUZOV, M. Z. & ONAEV, I. A. 1981. *Removal of impurities from lead*. SU patent application.

OKUNEV, A. I., CHUMAREV, V. M., SHOLOKHOV, V. M., SHASHMURIN, V. A., GUS'KOV, V. A., KIRYUSHKIN, B. N., DENISOV, V. I., ORLOV, A. F. & POTAPOV, M. V. 1975. *Processing of tin-containing iron-arsenic alloys*. SU patent application.

PEACOCK, M. A. & MCANDREW, J. 1950. Parkerite and shandite and the crystal structure of $Ni_3Pb_2S_2$. *Am. Mineral.,* 35**,** 425-439.

PELABON, H. 1905. Fusibility of Mixtures of the Antimony Sulfide with Copper Sulfide and Mercury Sulfide. *C. r. d. l'Acad. des sciences,* 140**,** 1389-1392.

PETERSON, M. & TWIDWELL, L. G. 1985. Removal of arsenic from lead smelter speiss. *J. Hazard. Mater.,* 12**,** 225-229.

POGUE, E. A., SUTRISNO, A., JOHNSON, N. E., GOETTER, M. B., JIANG, Z., JOHNSON, N. E., SHOEMAKER, D. P. & ROCKETT, A. A. 2019. Phase stability and structural comparison of phases in the Cu-Zn-Sn-S system using solid-state NMR. *Sol. Energy Mater. Sol. Cells,* 190**,** 37-48.

RUDNIK, E. 2016. Collection and recycling of spent nickel and lithium batteries and accumulators in Poland. *Metall. Foundry Eng.,* 42**,** 127-137.
SEITKAN, A., LAMPRONTI, G. I., WIDMER, R. N., CASATI, N. P. M. & REDFERN, S. A. T. 2020. Thermal Behavior of Iron Arsenides Under Non-Oxidizing Conditions. *ACS Omega,* 5**,** 6423-6428.
SHIMIZU, Y., YANO, T., SUZUKI, H., KOUNO, S. & IZUMI, T. 2003. Sol-gel processing and oxygen electrocatalytic properties of metal sulfides. *ITE Lett. Batteries, New Technol. Med.,* 4**,** 752-758.
SKINNER, B. J., LUCE, F. D. & MAKOVICKY, E. 1972. Studies of the Sulfosalts of Copper III. Phases and Phase Relations in the System Cu-Sb-S. *Econ. Geol.,* 67**,** 924-938.
SORULEN, T. T., TAKAHASHI, R., TANAKA, S., SUZUKI, K., IMAI, A., WATANABE, Y. & KIKUCHI, S. 2019. Mineralogical and Geochemical Characteristics of the Utanobori Gold Deposit in Northern Hokkaido, Japan. *Resour. Geol.,* 69**,** 402-429.
TOGUZOV, M. Z., NURBAEV, M., MINKEVICH, S. M., ZHAGLOV, V. S. & ONAEV, I. A. 1984. Physicochemical studies of the refining of lead by iron. *Kompleksn. Ispol'z. Miner. Syr'ya***,** 43-47.
TOMASHYK, V. 2022. *Ternary Alloys Based on IV-VI and IV-VI2 Semiconductors,* Boca Raton, CRC Press.
ZHENG, Y.-X., LV, J.-F., LAI, Z.-N., LAN, Z.-Y. & WANG, H. 2019. Innovative methodology for separating copper and iron from Fe-Cu alloy residues by selective oxidation smelting. *J. Cleaner Prod.,* 231**,** 110-120.